

Photoionising feedback in star cluster formation

J. E. Dale¹*, I. A. Bonnell², C. J. Clarke³ and M. R. Bate⁴

¹Department of Physics and Astronomy, University of Leicester, University Road, Leicester, LE1 7RH, UK

²School of Physics and Astronomy, University of St Andrews, St Andrews, Fife, KY19 9AJ, UK

³Institute of Astronomy, Madingley Road, Cambridge, CB3 0HA, UK

⁴School of Physics, University of Exeter, Stocker Road, Exeter, EX4 4QL, UK

25 June 2018

ABSTRACT

We present the first ever hydrodynamic calculations of star cluster formation that incorporate the effect of feedback from ionising radiation. In our simulations, the ionising source forms in the cluster core at the intersection of several dense filaments of inflowing gas. We show that these filaments collimate ionised outflows and suggest such an environmental origin for at least some observed outflows in regions of massive star formation. Our simulations show both positive feedback (i.e. promotion of star formation in neutral gas compressed by expanding HII regions) and negative feedback (i.e. suppression of the accretion flow in to the central regions). We show that the volume filling factor of ionised gas is very different in our simulations than would result from the case where the central source interacted with an azimuthally smoothed gas density distribution. As expected, gas density is the key parameter in determining whether clusters are unbound by photoionising radiation. Nevertheless, we find - on account of the acceleration of a small fraction of the gas to high velocities in the outflows - that the deposition in the gas of an energy that exceeds the binding energy of the cluster is *not* a sufficient criterion for unbinding the bulk of the cluster mass.

Key words: stars: formation, ISM: HII regions

1 INTRODUCTION

It has long been recognised that massive stars deposit considerable mechanical and thermal energy into the ISM by a variety of processes. On galactic scales, the main such feedback agent is supernova explosions (e.g. McKee & Ostriker 1977; Dekel & Silk 1986); however the relatively long time lapse before supernovae explode - compared with the dynamical timescale in star forming regions - ensures that supernovae are ineffective in regulating star formation in the close vicinity of the progenitor. At the opposite extreme of length scales, radiation pressure on dust operates in the region (a few hundred A.U. from a typical OB star) where dust is close to its sublimation temperature. This form of feedback is thus mainly instrumental in controlling the formation of the OB star itself (Wolfire & Cassinelli 1986, 1987; Yorke & Sonnhalter 2002; Edgar & Clarke 2003, 2004).

On intermediate scales (\sim parsecs), stellar winds and photoionisation are likely to play the primary role in regulating the formation of star *clusters* (e.g. Tenorio-Tagle et al. 1986, 1999, 2003). On the one hand, the star formation rate may be enhanced by the fragmentation of shells of dense gas

swept up by winds/expanding HII regions (e.g. Elmegreen 1998; Elmegreen et al. 2002; Whitworth & Francis 2002) but the acceleration and expulsion of gas from the neighbourhood of the OB star also ultimately limits the fraction of a molecular cloud core that can be turned into stars. This latter effect has important implications for the formation of bound star clusters, since - by simple energetic arguments - a cluster cannot remain bound if it rapidly loses more than 50% of its original mass (Hills 1980; Lada et al. 1984). (See also Goodwin 1997; Adams 2000; Geyer & Burkert 2001; Boily & Kroupa 2003, for more sophisticated analyses of this problem). Although the majority of stars form in clusters (Clarke et al. 2000), most of these clusters are already unbound at an age of $\sim 10^7$ years (Battinelli & Capuzzo-Dolcetta 1991). It is likely, at least in clusters that contain more than a few hundred members - and are thus populous enough to contain an OB star - that such feedback effects are decisive in unbinding nascent clusters.

Feedback is also likely to be the main factor that regulates the Galactic star formation rate (SFR). It has long been recognised that the observed SFR in the Milky Way of a few $M_\odot \text{ yr}^{-1}$ is only a few per cent of the value that would result if all the Giant Molecular Clouds (GMCs) in the Galaxy were turning into stars on their

* E-mail: Jim.Dale@astro.le.ac.uk (JED)

internal dynamical timescales (Zuckerman & Evans 1974). Although one solution is that star formation in GMCs is quasistatic - i.e. is regulated, perhaps by magnetic fields, so that it occurs on a timescale considerably longer than the dynamical timescale (e.g. McKee 1989) - recent re-appraisals of the characteristic lifetime of GMCs suggest that star formation is rapid but also swiftly terminated (Elmegreen 2000; Hartmann 2003). In this latter model, only a few per cent of the mass of a cloud ends up being incorporated into stars prior to its dispersal. Simple estimates - based on homogeneous molecular clouds - suggest that dispersal either by photoionisation (Whitworth 1979; Franco & Garcia-Segura 1996) or by OB stellar winds (Clarke & Oey 2002) would give rise to a star formation efficiency of this order.

To date, however, numerical feedback studies have been limited to the case of highly idealised cloud structures, i.e. smooth density profiles with spherical or axial symmetry (Yorke et al. 1989; Franco et al. 1990; Garcia-Segura & Franco 1996). Axisymmetric calculations demonstrate how feedback operates preferentially in directions of steeply declining density and suggest that the net effect of feedback in clouds that are realistically inhomogeneous may be very different from that in smoothed density fields. Although some consideration has been given to the propagation of radiation in inhomogeneous clouds (e.g. Hobson & Scheuer 1993; Hobson & Padman 1993; Witt & Gordon 1996; Röllig et al. 2002; Hegmann & Kegel 2003) - particularly with regard to explaining spatial variations in the abundances of photosensitive species - such calculations have not hitherto been combined with hydrodynamical star formation simulations. The reason for this is that radiation transport is most readily handled by Eulerian schemes, where it is relatively straightforward to perform integrals along optical paths. Such schemes are however challenged by the large density contrasts that develop in realistic star formation simulations, although Adaptive Mesh Refinement (AMR) methods are becoming an increasingly powerful tool in this regard (Tassis et al. 2003; Klein et al. 2003).

In this paper, we present pilot calculations of photoionisation feedback in SPH simulations of star cluster formation in realistically inhomogeneous clouds. (These simulations do not currently incorporate feedback from stellar winds, which may turn out to be a reasonable omission on the timescale of these simulations ($\sim 10^5$ years), since there is some suggestion that the youngest OB stars have anomalously weak winds; Martins et al 2004). Our calculations employ an algorithm for the inclusion of photoionisation in SPH. Briefly, this method locates the ionisation front at every hydrodynamical timestep and adjusts the temperature of the gas behind the front accordingly. The ionisation front is located by comparing the flux of ionising photons emitted in the direction of a given particle with the integrated recombination rate between the source and that particle. In this (Strömgren volume) technique, the integrated recombination rate is calculated *as though* the density structure between the particle and the source represented the radial variation of a spherically symmetric density distribution. Evidently this approach depends on the validity of the on-the-spot approximation (i.e. on the assumption that diffuse ionising

photons resulting from recombinations to the ground state are absorbed locally). Our method also implicitly assumes that the ionisation structure adjusts instantaneously to any changes in the gas distribution due to, for example, outflows. This assumption is valid provided that the timescale on which the gas distribution evolves is longer than the local recombination timescale, which is always the case in the simulations presented here. We note the generic similarity between the present algorithm and that proposed by Kessel-Deynet & Burkert (2000), inasmuch as both use the on the spot approximation and utilise the SPH neighbour lists to construct integrated recombination rates in an efficient manner; however, whereas Kessel-Deynet and Burkert evaluated the evolution of the ionisation fraction of each particle using time dependent ionisation equations, our method - by locating a Strömgren volume - assigns to each particle a wholly ionised or wholly neutral state at each timestep. The method turns out to be simpler and more robust than that of Kessel-Deynet and Burkert and is justified by the sharpness of the ionisation fronts in the high density environments we consider. A detailed description of the code and the results of one-dimensional tests will be published in a subsequent paper.

In reality, although the boundary of the HII region under such conditions is very sharp, the boundary between hot and cold gas is likely to be less so, since the non-ionising photons from the radiation source would produce a photo-dissociated region (PDR) outside the HII region, whose temperature might reach 1000 K (Diaz-Miller et al. 1998). The overall effect of this phenomenon is not easy to predict since, on the one hand, the smaller pressure gradient across the ionisation front will retard the HII region's expansion, but the additional thermal energy deposited over a greater volume of the cluster may increase the total mass involved in outflows. We do not treat PDRs in this work but the combined action of HII regions and PDRs would make an interesting subject of further study.

We also do not take into account the likely presence of dust in our HII regions. Wood & Churchwell (1989) found evidence of dust in *all* of the ultracompact HII regions in their survey and estimated that the dust was absorbing between 50 and 90% of the photon flux emitted by the source in each case. Considerable theoretical work has been done on the effect of dust on HII region evolution. Diaz-Miller et al. (1998) suggest that there exists an additional initial phase of HII region expansion in which the dust content of the ionised gas is either destroyed or expelled by the star's radiation field. Detailed numerical calculations by Arthur et al. (2004) suggest that Wood & Churchwell (1989)'s estimates of the fraction of ionising photons absorbed by dust were too large in most cases. In any case, reduction of the photon flux of a source by 90% results in a reduction in the size of the equilibrium Strömgren sphere by only about 50%. We therefore expect that inclusion of dust in our calculations would have little effect on our results, although it would probably increase the timescale for expansion of our HII regions somewhat.

For these pilot simulations, we plumb our photoionisation algorithm into the simulations of the formation of a massive star cluster by Bonnell & Bate (2002). Specifically, we introduce ionising radiation from a single source in the cluster core, ~ 1 initial free fall time after the

initiation of the collapse. For our present purposes, the important feature of the proto-cluster at the time that photoionisation switches on is that the gas distribution is highly inhomogeneous, with the cluster core lying at the intersection of several high density filaments which channel an accretion flow into the core. Although the Bonnell and Bate calculation is scale free (i.e. can be scaled to any system of isothermal gas containing the same number of initial Jeans masses in gas and the same number of point masses initially), the introduction of feedback necessarily introduces an absolute mass scale to the calculation. Our approach here has been to apply two different scalings to the Bonnell and Bate calculations, so as to explore the efficiency of feedback in relatively high and low density environments.

In Section 2 we describe briefly the calculations performed by Bonnell and Bate 2002 and the way in which we used these calculations to form the initial conditions for our study of photoionising feedback. In Section 3, we describe a high-resolution and a low-resolution calculation of a protocluster in which the gas densities were high ($10^5 - 10^9 \text{ cm}^{-3}$). In Section 4, we describe a single low-resolution calculation of a system with much lower gas densities ($10^3 - 10^6 \text{ cm}^{-3}$). In Section 5 we compare the two suites of simulations with simple one-dimensional calculations to assess the effect on the efficiency of feedback of the complex internal structure of our protoclusters and of the gravitational field of the ionising sources within them. In Section 6 we go on to draw conclusions.

2 INITIAL CONDITIONS

Feedback in all its forms is dominated by massive stars, so the study of the effects of feedback requires an understanding of the formation of high-mass stars. Although the formation of low-mass stars is moderately well-understood, the formation of high-mass stars is well known to be problematic. In particular, there has been considerable debate as to whether stars more massive than $\sim 10 \text{ M}_\odot$ can form by conventional accretion, due to the effect of radiation pressure on dust (Wolfire & Cassinelli 1986, 1987; Yorke & Sonnhalter 2002; Edgar & Clarke 2003, 2004).

Bonnell et al. (1998) proposed an alternative scenario for massive star formation, namely that massive stars form by the collision and merger of lower-mass stars. Bonnell & Bate (2002) explored this scenario by performing numerical calculations at two resolutions. The high-resolution calculation was run on the UKAFF facility at Leicester University, while the low-resolution run was conducted on a SUN workstation. Their initial conditions were a cluster containing 1000 M_J of isothermal gas and 1000 low mass stellar ‘seeds’ whose total mass corresponded to 10 percent of the gas mass and ≈ 9 per cent of the total mass of the system. They arranged the gas and stars in a spherically-symmetric Gaussian density distribution with zero velocity initially. Mergers between two stars were permitted if they approached each other within a distance of 10^{-5} times the initial cluster radius.

In both their calculations, Bonnell and Bate found that accretion increased the stellar density in the cluster

core enough to allow stellar collisions to occur, contributing in both simulations to the formation of a central object sufficiently massive to have a strong photoionising flux. In this paper, we take the end results (after about a freefall time) of their simulations as the initial conditions of our own calculations. At this point, about 7 per cent of the gas had accreted onto the stars, increasing the mean stellar mass by about 70 per cent. In addition, the mean stellar density increased by a factor of 10 and the maximum stellar density (defined by the minimum volume required to contain 10 stars) rose by a factor of $\simeq 10^5$. This proved to be sufficient to allow 19 stellar mergers and contributed to the formation of a very massive star in the cluster core. We emphasise that our choice of this system as a testbed for introducing photoionisation feedback is motivated largely by the fact that it shares several features with observed young clusters. In particular, we wish to explore conditions in which the ionising star is located near the cluster centre and in which the gas distribution is highly anisotropic.

We conducted three calculations, designated UH-1, SH-1 and SL-1. In all our calculations, we dispensed with stars and gas at large radii and rescaled Bonnell and Bate’s calculations by adjusting the length unit in the code to allow us to study two different regimes of behaviour. In UH-1 and SH-1, we study at two different resolutions virtually identical protoclusters whose gas densities are ($\sim 10^4 \text{ cm}^{-3} - \sim 10^8 \text{ cm}^{-3}$). UH-1 is based on Bonnell and Bate’s UKAFF run and SH-1 on their SUN run. In both of these calculations, we also rescaled the ambient temperature of the neutral gas to retain the absolute value of the Jeans mass. This resulted in ambient temperatures of $\sim 1.4 \text{ K}$, which are obviously unrealistically low, but we point out that varying the value of the ambient temperature by a factor of a few will have a negligible effect on the dynamical evolution of these calculations, since the behaviour of the protoclusters will be dominated by the thermal pressure of the hot ionised gas and the ram pressure of the accretion flows, both of which are several orders of magnitude greater than the ambient thermal pressure even before rescaling. These calculations are described together in Section 3.

In SL-1, also based on Bonnell and Bate’s SUN run, we simulate a protocluster with somewhat lower gas densities ($\sim 10^3 \text{ cm}^{-3} - \sim 10^6 \text{ cm}^{-3}$). We elected not to rescale the ambient temperature in this calculation, instead leaving it at 10 K . This calculation is described in Section 4. In all calculations, we used our Strömgren volume technique to define the HII region at each hydrodynamic timestep, heating the gas within to $10,000 \text{ K}$. The properties of our three model clusters are given in Table 1.

3 SIMULATIONS OF HIGH-DENSITY INITIAL CONDITIONS

We describe the UH-1 and SH-1 runs together in this section since they are essentially simulations of the same protocluster differing only in their numerical resolution. In common with Bonnell & Bate (2002), we conducted our high-resolution UH-1 simulation on the UK Astrophysical Fluids Facility’s SGI Origin 3800 and the corresponding

	UH-1 run	SH-1 run	SL-1 run
Particle number	5×10^5	5×10^4	5×10^4
Total mass (M_\odot)	742	745	745
Initial stellar mass (M_\odot)	225	223	223
Initial gas mass (M_\odot)	517	522	522
Initial radius (pc)	1.4	1.4	2.8
Initial Jeans mass (M_\odot)	0.8	0.8	40.5
Core gas density (cm^{-3})	$\sim 10^9$	$\sim 10^8$	$\sim 10^6$
Mean gas density (cm^{-3})	$\sim 10^4$	$\sim 10^4$	$\sim 10^3$
Freefall time (yr)	1×10^6	1×10^6	2×10^6
Source luminosity (s^{-1})	6×10^{49}	6×10^{49}	2×10^{49}

Table 1. Parameters of our runs. All gas densities quoted are atomic hydrogen number densities.

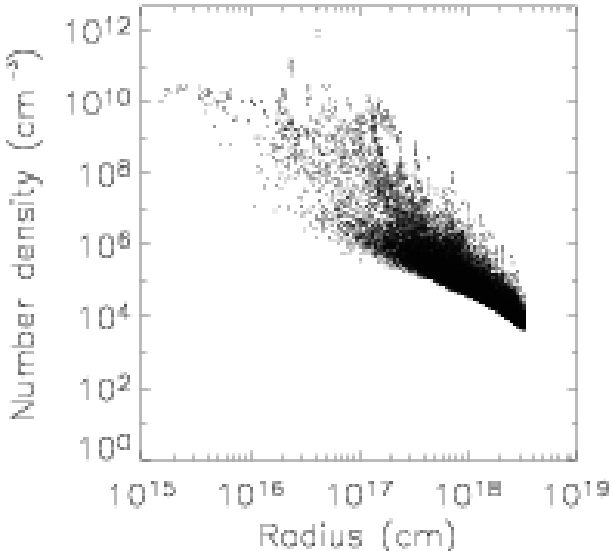


Figure 1. Initial radial density profile of the UH-1 calculation. Only every tenth particle has been plotted.

low-resolution one on a SUN workstation. The initial conditions for the UH-1 and SH-1 simulations, given in Table 1, were quantitatively almost identical. The ionising source in these calculations has an initial mass of $\sim 30 M_\odot$. We regard it as a point source of ionising photons and assign to it an ionising flux of $6 \times 10^{49} \text{ s}^{-1}$. This is a rather generous output even for such an O-star ($2 \times 10^{49} \text{ s}^{-1}$ would be more realistic), but is justified, since the ionising star in these simulations grows considerably in mass (to a few $\times 100 M_\odot$) through further accretion (see Diaz-Miller et al. (1998) for a table of O-star ionising luminosities). We note that this luminosity is close to the source's classical Eddington luminosity, but accretion continues along the gaseous filaments, since the inhomogenous structure of the gas increases the source's effective Eddington luminosity (see Shaviv (2001) for a discussion of super-Eddington accretion in inhomogenous environments).

3.1 The UH-1 run

In Fig. 1, we plot the initial radial density profile of the UH-1 protocluster. There is clearly an enormous range of gas

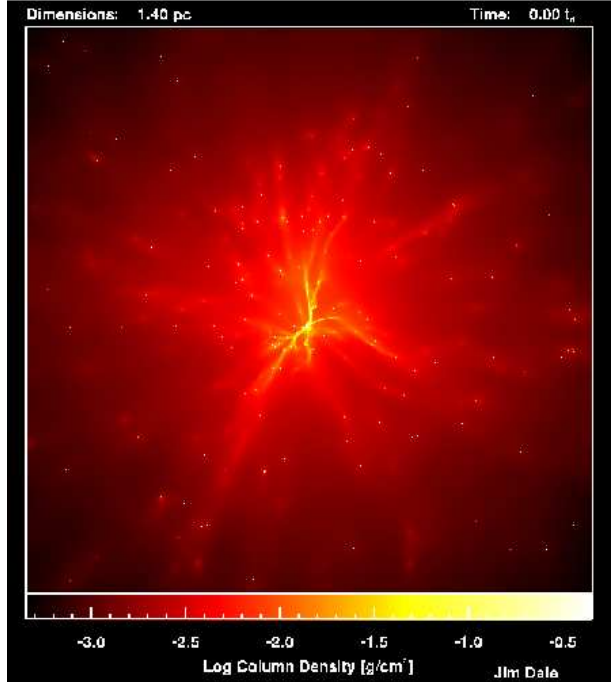


Figure 2. Column density map of the inner $1.4 \text{ pc} \times 1.4 \text{ pc}$ of the initial conditions for our UH-1 calculation as viewed along the z -axis.

densities in the system. The profile approximately follows a power-law with slope $\alpha \approx -2$, but there is evidently a great deal of substructure superposed on this general configuration. This can be seen in detail in Fig. 2 which shows a column-density map of the protocluster (the ionising source is at the centre of the image).

It can be seen that the initially-smooth gas in Bonnell and Bate's original calculation has developed a complex filamentary structure which approximately radiates outwards from the core. The distribution of residual gas closely follows that of the stars, with stars being preferentially located inside gaseous filaments. These structures are due to gravitational instabilities in the gas which amplify pre-existing shot noise in the stellar seed distribution. One of the aims of this study is to see what effect this structure has on the efficacy of feedback.

The gas is distributed highly anisotropically with respect to the O-star at the centre of the protocluster. Figure 3 shows a θ, ϕ column density map of the cloud as seen from the ionising source. One expects that this structure will result in the distance to which ionising radiation can penetrate the protocluster to be similarly anisotropic and our simulations demonstrate that this is true.

We found that ionising radiation is able to escape from the immediate vicinity of the massive star in only a few directions, forming several outflows and corresponding elongated HII regions. The radiation and thus the outflows are loosely collimated by the dense gas near the star. By restricting the directions in which radiation can escape from the source, a small mass of gas distributed very close to the ionising source is able to dominate the evolution of the ionised region and thus to control its effect on the rest of the cloud. Bonnell and Bate suggested such collimation as a

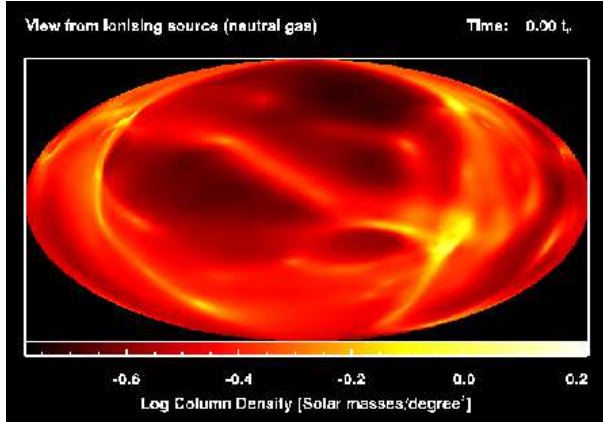


Figure 3. θ, ϕ column density map of the gas distribution in the UH-1 cluster at the beginning of the simulation as seen from the ionising source. Only material within 0.2 pc has been included in this map in order to emphasise the anisotropic conditions encountered by the source's radiation field.

possible explanation for the poorly-collimated outflows observed around young massive stars. This work lends considerable support to this proposal. However, we note here that this collimation may be due in part to noise in the particle distribution close to the source, since a single particle at a small radius is potentially able to shield a large number of particles further out in the cloud. This importance of this effect could be studied by splitting gas particles close to the source into ~ 10 (for example) smaller, lower-mass particles, but the presence of particles of very different masses in the same region of space can give unphysical results in SPH. We have not investigated this issue.

The end result of our calculation is shown in Fig. 4 at which point the ionising source has been radiating for $\sim 1.7 \times 10^5$ yr, $\sim 17\%$ of the cluster's global freefall time.

3.1.1 Outflows

The outflow structure is evidently very complex. Watching an animation of the simulation allows six or seven individual radial flows to be identified. These outflows are visible as the dark regions in Figure 5, a second θ, ϕ plot of the gas column density seen from the source, generated at the same epoch as Fig. 4. The disposition of the outflows is interesting in that they are all confined to the left-hand half of the cloud. Hence, the left hemisphere of the cloud has a radically different structure by the end of the calculation, whereas the right hemisphere is almost untouched.

The outflows are weakly collimated. Their opening angles can be estimated by eye from Figure 5 and are approximately $10^\circ - 20^\circ$. The ionised gas in the outflows expands azimuthally as well as radially, sweeping up neutral material and generating numerous fresh filamentary structures, particularly where neutral gas is caught between two expanding bubbles. These filaments are also visible in Fig. 5 as the narrow bright features within the dark areas of the plot. The filamentary structures subsequently fragment into strings of clumps whose densities increase with time, as they are immersed in hot ionised gas and are therefore un-

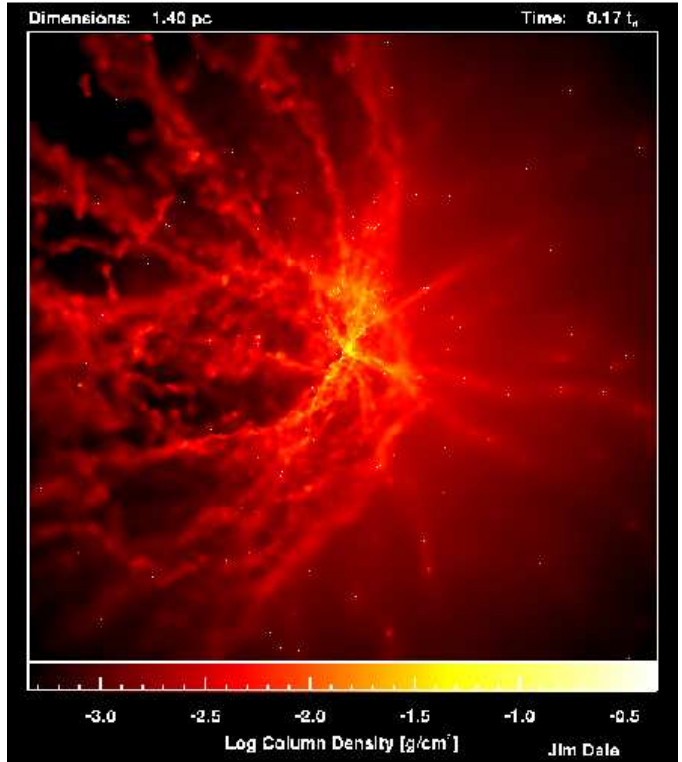


Figure 4. Column density map showing the end result of the UH-1 calculation after $0.17 t_{ff}$, as viewed along the z -axis. Note the asymmetric distribution of the outflows.

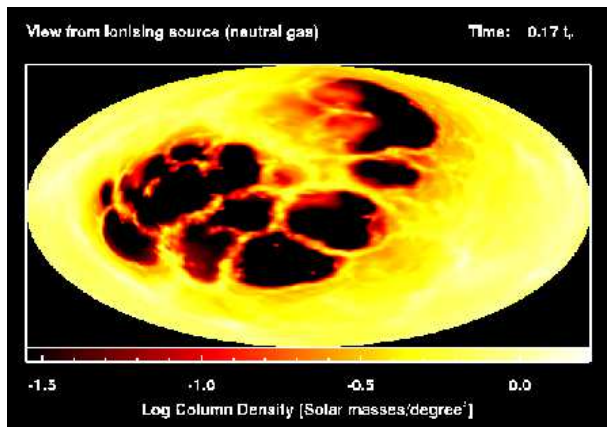


Figure 5. A θ, ϕ column density map of the neutral gas distribution as seen from the source in the UH-1 calculation at $t = 0.17 t_{ff}$. All neutral gas has been included in this map.

der strong compression. At the point where we were forced to stop the simulation, the entire left-hand hemisphere of the protocluster is a chaotic assembly of chains of isolated clumps and filaments still in the process of subfragmentation. The right-hand hemisphere of the cloud remains largely untouched because of shielding by very dense material just to the right of the ionising source. It can be seen in the animation that the source is beginning to clear away this material and it is likely that the protocluster would become more homogeneous if it were possible to continue the simulation. However, we were forced to terminate the simulation

prematurely because numerous particles acquired timesteps which were prohibitively short, slowing the calculation dramatically. This is due to the development of strong density enhancements owing to the increased fragmentation.

We compare the mass entrained in the outflows and the momentum this mass carries with outflows observed in real star-forming regions. In Fig. 6, we plot histograms showing the masses of gas involved in inflows and outflows at the beginning and at the end of the simulation. Initially, most of the gas in the system is infalling at speeds of 5 km s^{-1} or less. The outflows are clearly visible in the overlaid later plot as material with high positive radial velocities. The total mass involved in the outflows is $\sim 30 M_{\odot}$, about seven percent of the total gas mass. Only about one third of the gas involved in the outflows is ionised, the remainder being swept-up neutral gas. The mean rate at which the outflows are removing mass from the cluster core is $\approx 2 \times 10^{-4} M_{\odot} \text{ yr}^{-1}$. The total outflow momentum is $\approx 10^3 M_{\odot} \text{ km s}^{-1}$, in good agreement with observed values as tabulated by Churchwell (1997) for stars in the spectral range B0-O4.

Although this agreement with the parameters of observed outflows is encouraging, we note here that the outflows in our simulations, which are driven by anisotropic heating, are not in general bipolar in nature, since their number and symmetry is determined purely by details of the initial gas structure near the radiation source. At first sight, this would appear to disfavour such a mechanism since outflow sources from young massive stars are usually described as being bipolar (e.g. Kumar et al. 2002; Beuther et al. 2002). However, as noted by Shepherd et al. (1997), this designation can be misleading, since outflow lobes may not be symmetric and some outflows appear to be monopolar. The outflows described here clearly cannot be compared to the highly-collimated sources recently discovered in pre-UCHII regions (Beuther et al. (2002), Davis et al. (2004)) but they may be compatible with some of the less collimated objects described by Shepherd et al. (1997). It is currently unclear what fraction of observed outflows could be explained by the mechanism we discuss here, and what fraction require the conventional scenario of bipolar flows emanating from an accretion disc.

3.1.2 HII regions

The structure and behaviour of the ionised gas in this simulation is unusual for two reasons. Firstly, the HII region possesses a multi-lobed structure due to the beaming effects mentioned in the preceding paragraphs. An example is shown in Figure 7, showing clearly that the HII region(s) generated in these calculations bear little resemblance to the classical picture of the Strömgren sphere. Although unusual, the HII region depicted in Figure 7 is in appearance not unlike some of the ‘cometary’ ultracompact HII regions described in Wood and Churchwell’s seminal paper on the subject (Wood & Churchwell 1989), in particular G29.96-0.02 (shown on page 863 of Wood & Churchwell (1989)) and G43.89-0.78 (shown on page 867).

The second unusual property of our HII regions is their variability. In the early stages of the simulation, the HII regions are observed to ‘flicker’ on short timescales (a few hundred to a few thousand years), frequently disappearing completely, only to regrow a short time later. This can be

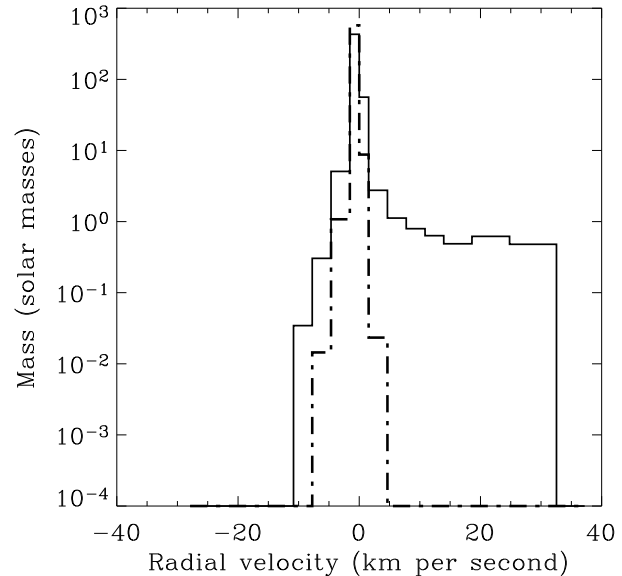


Figure 6. Histograms showing the initial distribution of velocities with mass (dotted lines) and the final distribution including the outflows driven by the thermal pressure of the ionised gas in the UH-1 calculation, as described in the text (solid lines).

seen in Fig. 8 where we plot the fraction of the protocluster’s gas which is ionised as a function of time. Although the general tendency is for the ionisation fraction to increase, it exhibits numerous sharp rises and falls, particularly in the early stages of the calculation.

Figure 8 implies, particularly in the early stages of the simulation, that the HII region contains small numbers of SPH particles, sometimes below the canonical resolution limit of ~ 50 , corresponding to a particle and its neighbours. We conducted convergence tests in a uniform spherically symmetric model cloud to determine what effect such apparent under-resolution might have on the expansion of the HII regions in our simulations. We found that we were able to reproduce the well-known Spitzer solution for the expansion of a spherical HII region in a uniform cloud (Spitzer (1978)) even when the HII region initially contained as few as three (!) SPH particles. We concluded from this that the resolution requirements pertinent to modelling the expansion of HII regions are rather less stringent than those relevant to other physical processes, although clearly the accuracy with which the detailed geometry of HII regions can be modelled is dependent on the available resolution.

The cause of the flickering behaviour is the rapid and non-uniform accretion taking place in the core of the protocluster, mostly along the dense filaments. Although, in the simulations, this effect is partly shaped by finite resolution near the source (i.e. the effect of individual SPH particles), it is more generally the case that small fluctuations in the amount of neutral matter near the source can have a profound effect on the propagation of ionising radiation to large radii. At early times, the interplay of the expanding HII regions and the accretion flows results in the source region being intermittently inundated by inflowing neutral gas on a characteristic timescale similar to the freefall timescale in the cluster core. Since this timescale is long compared with the recombination timescale anywhere in

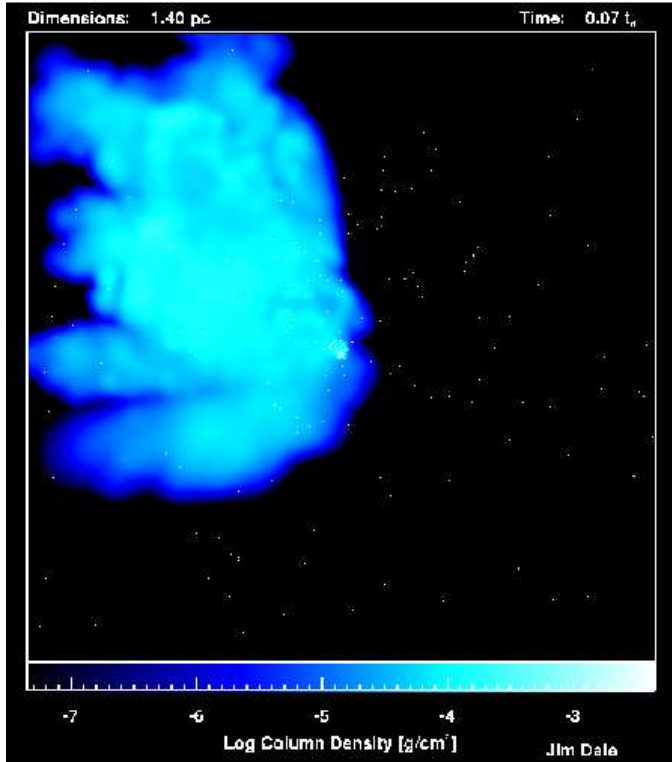


Figure 7. Column density map of the ionised gas in the UH-1 simulation $0.07 t_{ff}$ after source ignition revealing the unusual shape of the HII region.

the cluster, the HII regions are able to respond by switching on and off on this timescale (see Figure 8). However, after about 10^5 yr, a quasi-steady flow pattern is set up, in which the neutral flow never completely swamps the core region and the mass of ionised gas thereafter grows steadily with time.

Once the HII region has reached its stable phase, it is able to have a dramatic effect on the structure of the gas in the protocluster, since ionised gas is able to permeate a significant fraction of the cluster's volume (although the ionisation fraction in this simulation was never more than three percent). We observed the emergence of a great deal of novel structure, but we were not able to follow the protocluster's evolution long enough to study the gross dynamical effects of photoionising feedback. We therefore turn to the low-resolution SH-1 calculation which was able to run for somewhat longer.

3.2 The SH-1 run

The SH-1 calculation was started from similar (although not identical) initial conditions to those of the UKAFF run and was able to continue for considerably longer, allowing us to study the long-term dynamical impact of the HII region on our protocluster and to determine the effect of the fragmentation process observed in the high-resolution run on the star formation within the cloud. The initial conditions for this calculation are shown in Fig. 9. They are clearly qualitatively similar to those of the high-resolu-

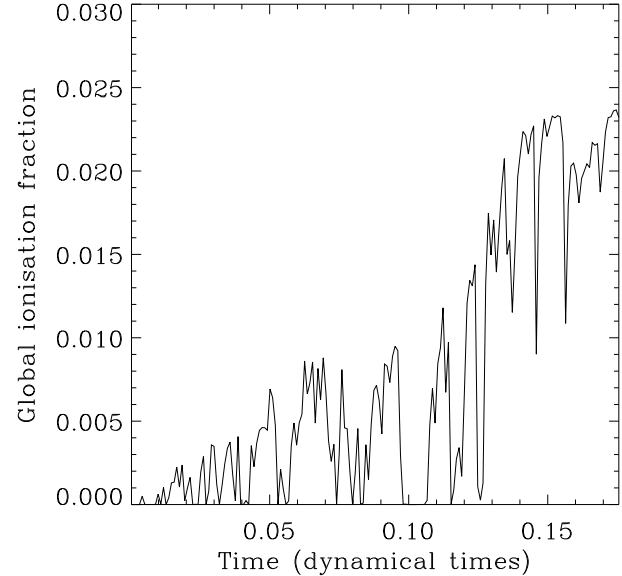


Figure 8. A plot of the UH-1 protocluster's global ionisation fraction as a function of time, revealing the flickering process described in the text. The dynamical time of the system is 10^6 yr.

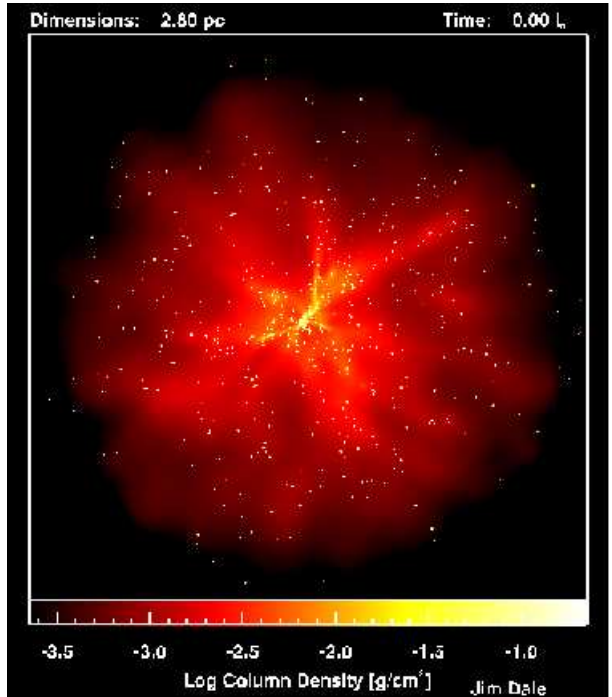


Figure 9. Column density map of the initial conditions for our SH-1 calculation as viewed along the z -axis.

run, as can be seen by comparing Figures 2 and 9.

The evolution of the low-resolution simulation was similar to the UKAFF calculation, as shown in Figure 11. We again observed several weakly-collimated outflows driving bubbles of ionised gas into the protocluster's ambient neutral gas, generating filamentary and beadlike structures as they went. We also observed the phenomenon of HII-region flickering, depicted in Figure 10, again dying away as the ionising source was able to expel some of

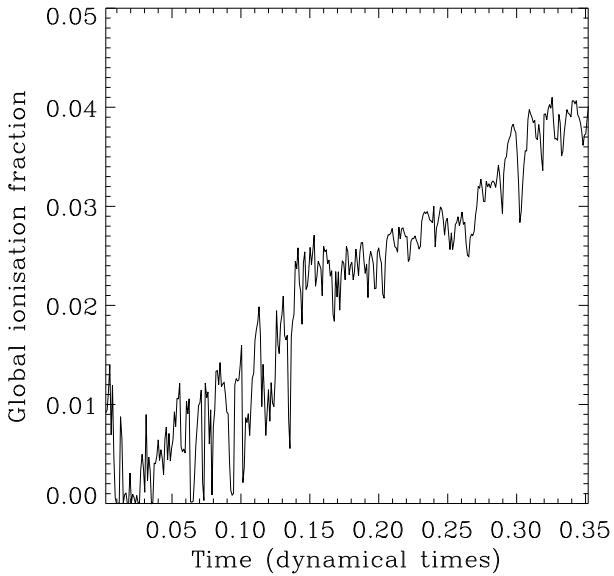


Figure 10. A plot of the global ionisation fraction as a function of time for our SH-1 calculation. As in the UH-1 run, we observe that the HII region initially flickers rapidly before settling down to a stable expansion phase. The dynamical time of the system is 10^6 yr.

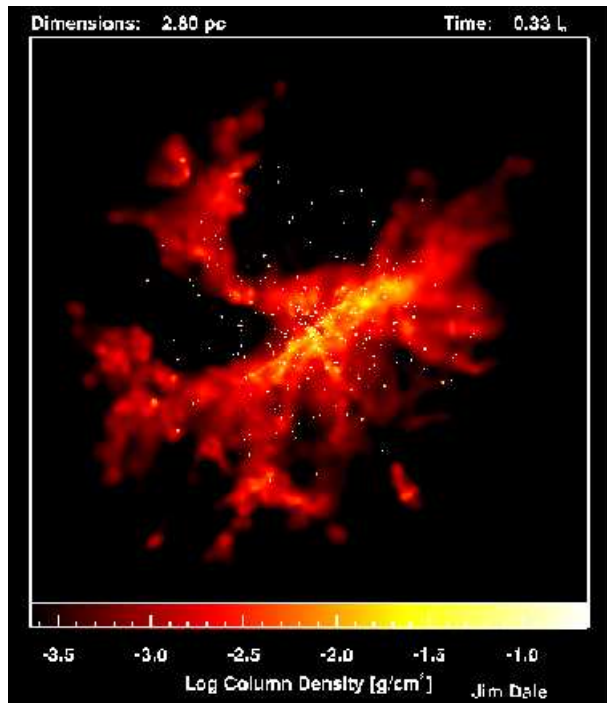


Figure 11. Column density map of the end result of the SH-1 calculation after $0.33 t_{ff}$, as viewed along the z -axis.

the dense gas from its immediate vicinity and deflect the accretion flows away from the core. However, in this case, we are more interested in the later evolution of the system.

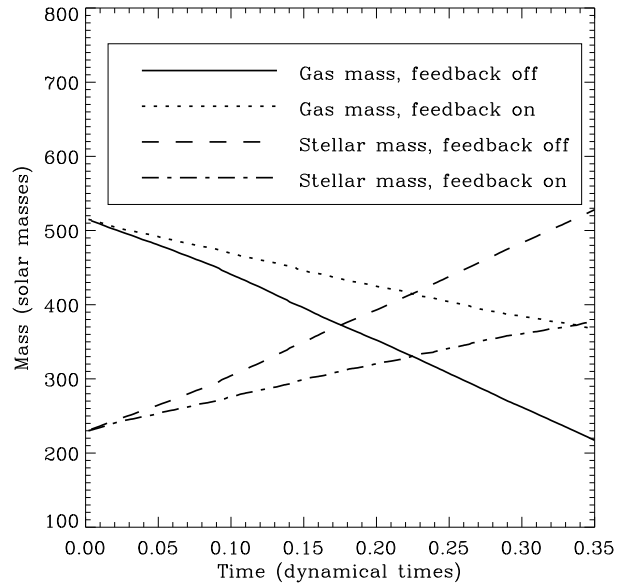


Figure 12. Comparison of the evolution of the masses of the SH-1 cluster's stellar and gaseous components in runs with feedback active and inactive. The dynamical time of the system is 10^6 yr.

3.2.1 Accretion, energy uptake and cluster survival

The most obvious question to ask is whether the radiation from our massive star is able to prevent the cluster from becoming permanently gravitationally bound. At the beginning of our simulations, the cluster is bound, but the ratio of gas mass to stellar mass is $\sim 2.5 : 1$, so rapid expulsion of significant quantities of gas could unbind the cluster. Since accretion is still in progress in the core of the cluster, this ratio is clearly approaching $1 : 1$ as time progresses. If the ratio of gas mass to stellar mass reaches $1 : 1$ while the system is still globally bound, the cluster, or at least its stellar content, will remain bound regardless of what happens to the remaining gas. The question of whether feedback can unbind the cluster therefore reduces to seeing if the accretion flows can be stopped before this occurs. In Fig. 12, we show how the total masses of the stellar and gaseous components of the protocluster evolve with time in the SH-1 calculation. We compare the SH-1 calculation with another one identical except that the ionising source was left switched off. In both plots, all the gas and all the stars in the clusters are included whether still bound to the cluster or not, so the change in the masses of the two components is due purely to accretion.

The global accretion rates in the two simulations are given by the gradients of the lines in Fig. 12. The accretion rate in the case with feedback active is lower than in the run without feedback but accretion is never halted because the thermal pressure of the ionised gas is considerably less than the ram pressure of the accretion flows. The stellar and gas masses reach equality at a later time with feedback active but examination of the energies of the cluster's stellar and gaseous components revealed that all the stars and $\sim 83\%$ of the gas are still bound at this point in time, so photoionising feedback has failed to unbind the cluster.

We now compare the stellar energy input with the thermal and kinetic energies of the gas to see how efficiently the

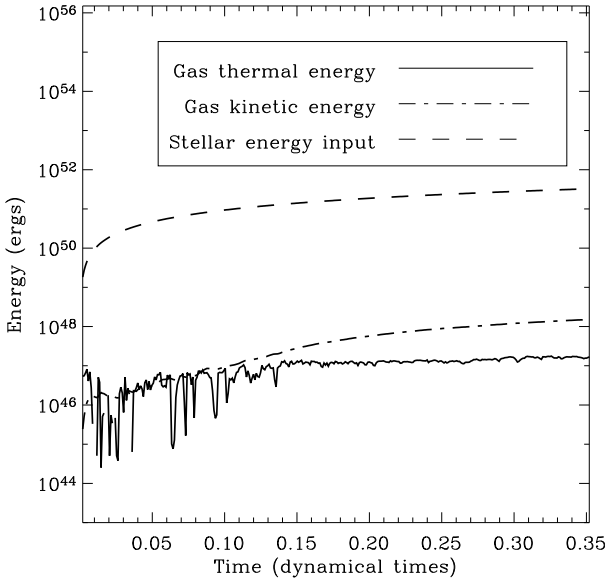


Figure 13. Comparison of the stellar energy input with the gas thermal and kinetic energies in the SH-1 calculation. The dynamical time of the system is 10^6 yr.

energy emitted by the ionising source is being taken up by the system and we compare the total energy uptake with the cluster's gravitational self-energy. The gravitational potential energy of an object of mass M and radius r is given approximately by

$$E_{grav} \simeq \frac{GM^2}{r} \quad (1)$$

Our protocluster has a total mass of $740 M_\odot$ and a radius of 4.2×10^{18} cm, giving $E_{grav} \simeq 3 \times 10^{46}$ erg. In Fig. 13, we plot the gas thermal and kinetic energies against time along with the energy input by the star since its ignition (taking this to be the energy contained in 6×10^{49} 13.6 eV photons $s^{-1} \times$ (time since ignition)). Two things are immediately apparent from Fig. 13: firstly, the photoionisation process in this cluster is extremely inefficient, with $< 0.1\%$ of the energy injected by the star being retained. We have assumed that all recombinations of ions with electrons that initially deposit the electron in an atomic energy state other than the ground state result in the emission of a photon or a series of photons to which the gas is optically thin. Such recombinations therefore constitute an energy sink. In addition, at the end of the calculation, $\sim 20\%$ of the ionising flux is escaping from the cloud directly, through holes in the gas distribution.

Secondly, despite the inefficient coupling, the star apparently *has* deposited enough energy into the gas to unbind the cluster as a whole.

This leads to the obvious question of why the cluster does not become globally unbound. The answer is simply that, although sufficient energy has been absorbed by the cluster gas to exceed the cluster's total gravitational binding energy, this energy is distributed throughout a small proportion ($\sim 17\%$) of the gas. As can be seen in Fig. 14, the ionised gas is escaping from the cluster, entraining some neutral gas with it, and carrying thermal and kinetic energy away, so this energy has little effect

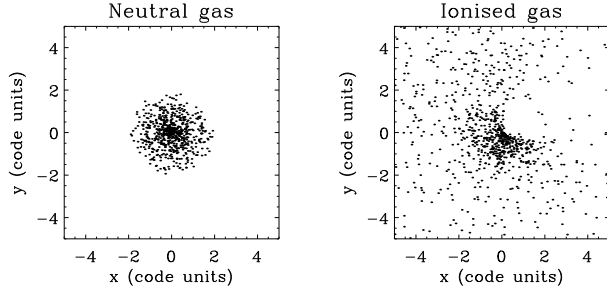


Figure 14. xy-plots of the positions of neutral and ionised gas particles in the SH-1 run, revealing that the hot ionised gas is able to effectively escape the protocluster.

on the cloud as a whole. Although the energetic material becomes unbound, the remainder, constituting over 83% of the cluster's gaseous component, is still firmly bound within the cluster's gravitational potential well.

Our neglect of the likely existence of a PDR outside the HII region in these calculations clearly affects the energetics of our cluster. The presence of a PDR would result in the thermal energy of the cluster gas being higher and may also increase the kinetic energy of the gas by involving a larger fraction of it in outflows. However, the results presented in this section suggest that *where* in the cluster thermal energy is deposited is at least as important as the bare quantity of energy. The expansion of the HII region in this protocluster was controlled by the dense material and accretion flows near the radiation source and it is likely that the PDR would be similarly constrained. We think it unlikely that modelling the PDR would substantially alter our conclusions.

3.2.2 Star formation

In none of our simulations was the mass resolution good enough to follow the star formation process in detail, but we can draw qualitative conclusions about the effect of feedback from the evolution of the cluster's mean Jeans mass, depicted in Figure 15, where we have again made a comparison with the control simulation without feedback. In both cases, the mean Jeans mass was estimated using the mean density of the *neutral* component of the cluster gas only, comprising not less than 95 per cent of the total gas mass of the feedback (and 100 per cent of that in the control run), taking the neutral gas in both runs to have the initial ambient temperature. The evolution of the mean Jeans mass in the two systems is initially similar, but becomes very different after $\sim 0.1 t_{ff}$. Although both plots exhibit rapid fluctuations, the general trend in the control run is for the Jeans mass to increase, whereas in the feedback run, the Jeans mass decreases. The former result is somewhat counterintuitive: since the system is collapsing unimpeded, one might expect the mean gas density to rise and the Jeans mass to fall (given that the temperature is constant). However, because of the rapid accretion taking place in the control simulation and because high-density gas in the cluster core is accreted more rapidly than low-density gas further out in the cluster, the mean gas density in this calculation actually *decreases* overall.

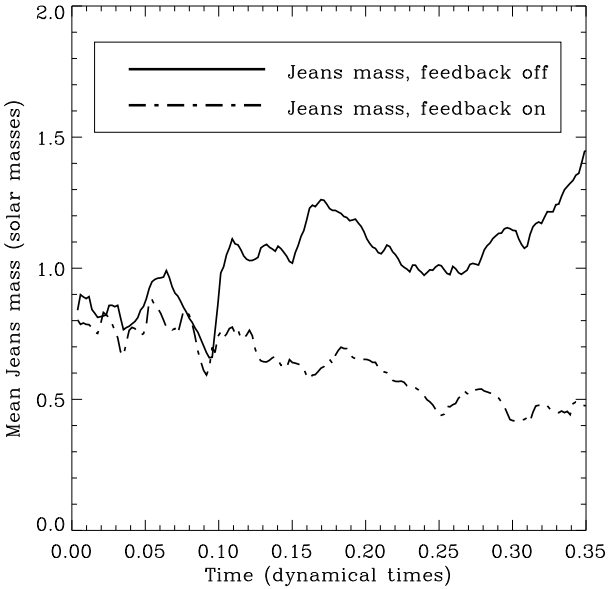


Figure 15. Evolution of the mean Jeans mass within the SH-1 cluster. The dynamical time of the system is 10^6 yr.

In the feedback calculation, the accretion rate is considerably lower, as shown in Figure 12 and it is in the core that the accretion rate is most affected. In addition, the spread of hot ionised gas throughout much of the cluster's volume results in the compression and fragmentation of much of the system's remaining neutral gas - this process can be clearly seen in Figure 4 by comparing the highly-fragmented left-hand-side of the cloud with the almost-untouched right-hand side. The net result of these effects is that the mean gas density in the feedback calculation *increases*, driving the Jeans mass down (non-monotonically) from its initial value of $\approx 0.8 M_\odot$ to $\approx 0.4 M_\odot$. Although the mass resolution of the calculation ($\sim 0.5 M_\odot$) is not sufficient to follow the fragmentation/star-formation process (and indeed only a few new stars were observed to form during the simulation), we can infer from this plot that the overall effect of the ionising source is to decrease the protocluster's mean Jeans mass and thus to promote fragmentation. We cannot, however, make any statements regarding how many new stars will actually form.

4 SIMULATIONS OF LOW-DENSITY INITIAL CONDITIONS

In the previous section, we studied a cluster in which the feedback effects of the massive stars were strongly constrained by the physical structure and dynamical properties of the gaseous component of the system. We now consider a protocluster in which the gas density is approximately an order of magnitude lower and on which we therefore expect feedback to have a greater impact.

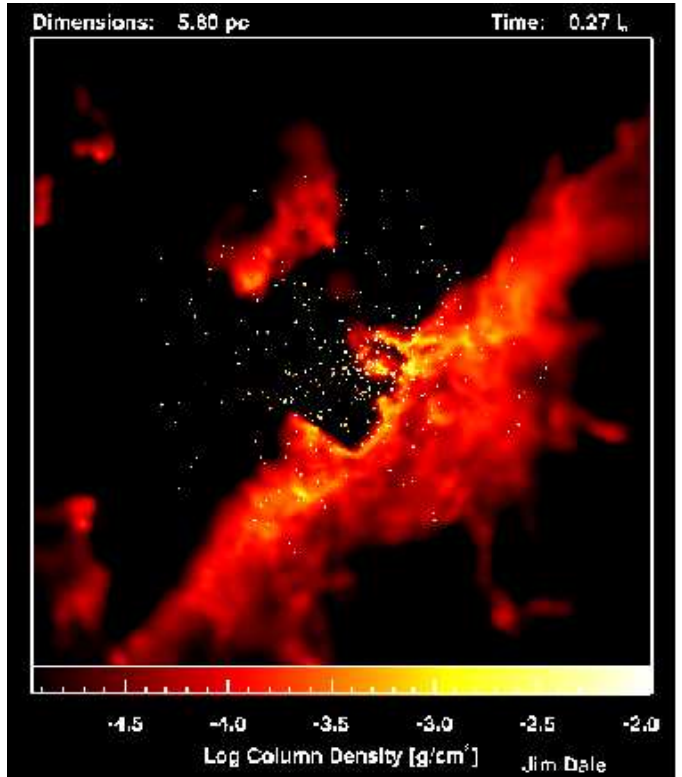


Figure 16. Column density map of the end result of the SL-1 run after $0.27 t_{ff}$, as viewed along the z -axis.

4.1 The SL-1 run

In our SL-1 simulation, we study a cluster in which the gas density is considerably lower (as we have increased the physical size of the cluster), in an attempt to give feedback an opportunity to have a greater influence on the protocluster's dynamical evolution. The ionising source in this simulation had an initial mass of $\sim 30 M_\odot$, rising to $\sim 60 M_\odot$ by the end of the run. It was assigned an ionising photon flux of $2 \times 10^{49} \text{ s}^{-1}$.

4.1.1 Accretion, energy uptake and cluster survival

The evolution of this simulation is markedly different from that of either of the foregoing calculations. Fig. 16 shows a column-density map of the end result. Although superficially similar to Fig. 11, careful inspection shows that photoionisation has been more successful in expelling gas from the core of the protocluster in the low density simulation. As can be seen by close examination of Figs. 11 and 16, there is a higher degree of segregation between the stars and the gas in the SL-1 simulation and this has been achieved on a shorter timescale than in the SH-1 calculation. Because of the lower gas densities in the SL-1 system, the radiation source is able to partially ionise and thus disrupt the radial accretion flows. Fig. 17 shows a plot of the global ionisation fraction in the SL-1 run. Although the flickering phenomenon observed in the UH-1 and SH-1 calculations does occur in this run, it dies away much more rapidly, allowing the ionisation fraction to rise more monotonically and

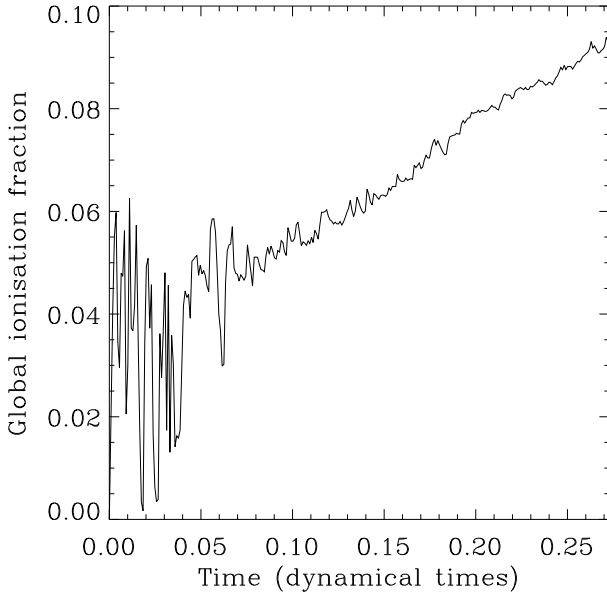


Figure 17. Evolution of the global ionisation fraction in the SL-1 calculation. The dynamical time of the system is 2×10^6 yr.

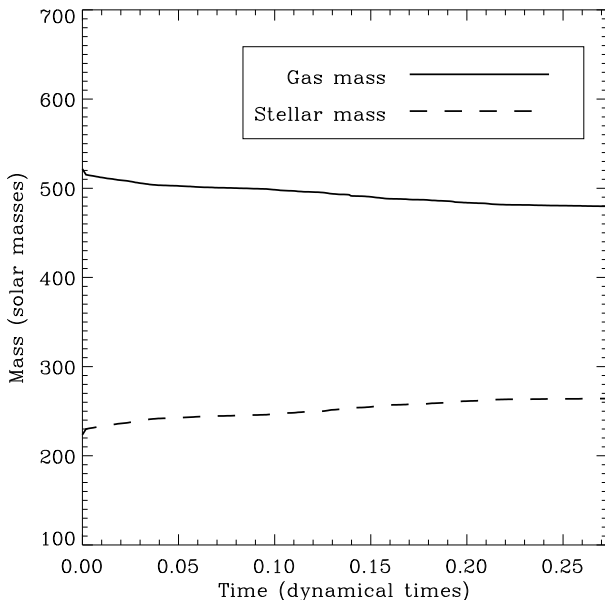


Figure 18. The accretion behaviour of the SL-1 calculation. The dynamical time of the system is 2×10^6 yr.

to attain higher values, although only by a factor of a few. The disruption of the accretion flows has the natural consequence that the global accretion rate in the SL-1 run is lower. Figure 18 shows that feedback quickly brings accretion to an almost complete halt, leaving the stellar:gas mass ratio little changed from its initial value.

As shown in Figure 19, the energy transfer in this calculation is somewhat more efficient than in the SH-1 simulation, despite the fact that $\sim 70\%$ of the ionising flux is escaping from the system at the end of the run. In addition, the gravitational binding energy of this system is somewhat lower ($\sim 10^{46}$ erg), so the SL-1 protocluster is ‘easier’ to unbind. This is reflected in the dynamical end-states of the

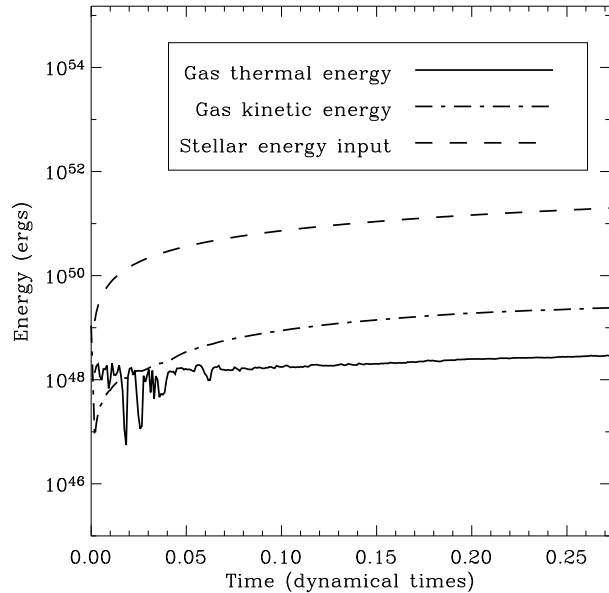


Figure 19. Comparison of the stellar energy input with the gas thermal and kinetic energies in the SL-1 run. The dynamical time of the system is 2×10^6 yr.

calculations. In the SH-1 calculation, the fraction of gas still gravitationally bound at the ‘point of no return’ where the total stellar mass comes to exceed the total gas mass was 83% and accretion was still in progress, so the SH-1 protocluster was almost certain to remain globally bound. By contrast in the SL-1 protocluster, accretion is almost halted by feedback and the bound gas fraction drops to less than 65% by the end of the simulation, ~ 0.27 freefall times after source ignition. 5% of the stars are also unbound at this point. We expect the fraction of unbound stars to rise as more gas is expelled from the system, but it is not possible to say on the basis of this calculation whether any of the cluster’s stellar population will remain bound.

As in the SH-1 simulation, the energetics of this system have been modelled ignoring the likely existence of a PDR surrounding the HII region which would result in the deposition of a larger quantity of thermal energy in the gas and over a larger volume. It is probable that modelling this effect would lead the SL-1 protocluster to become unbound faster but, again, we do not feel that our conclusions would be significantly different.

4.1.2 Star formation

We qualitatively assess the impact of feedback on star formation in the SL-1 cluster by examining the evolution of the mean Jeans mass, again estimated using the mean density of the protocluster’s *neutral* gas content only and taking its temperature to be the initial ambient temperature. The result is shown in Figure 20. After approximately $0.05 t_{ff}$, the mean Jeans mass increases sharply by about fifty percent. This is due destruction of dense filaments of neutral gas near the radiation source by expanding ionised gas. Although this process continues throughout the calculation, it is counterbalanced by the compression of neutral gas further out in the protocluster as it is swept

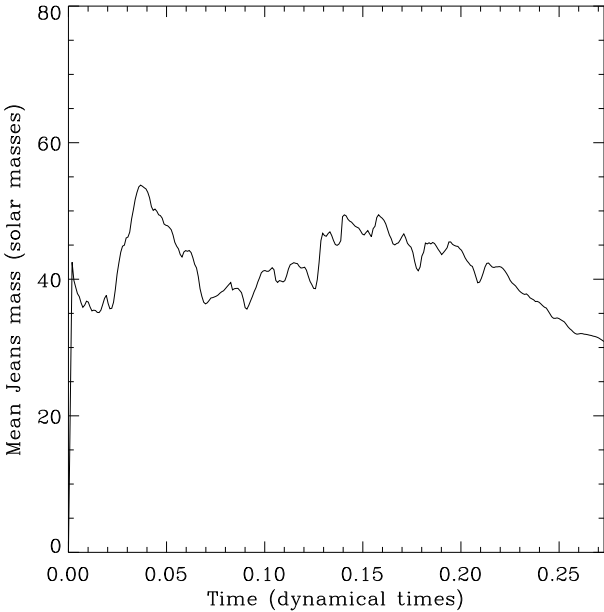


Figure 20. The evolution of the mean Jeans mass in the SL-1 calculation.

up by the growing HII region. Comparison of the SH-1 and SL-1 calculations reveals that feedback has two competing effects on the gas in protoclusters. Which effect dominates is determined by the gas density of the system. Feedback can decrease the gas density in the cluster core by destroying the structure there, but this effect was not observed in the high-density calculations because this material was simply too dense. Conversely, feedback can raise the gas density in the outer reaches of the cluster by sweeping up neutral gas and generating new structure. This latter effect dominated in UH-1 and SH-1 calculations, driving the global mean gas density up and the mean Jeans mass down. In the SL-1 calculation, the two effects roughly cancel each other for most of the run and the mean Jeans mass changes little. However, after $0.2 t_{ff}$, disruption of the dense structure in the SL-1 cluster core is complete and compression of material further out in the cluster begins to dominate. The impact of feedback on the star-formation process in this system is less clear-cut than in the previous simulations but, in the later stages of the calculation, feedback is again aiding the fragmentation process. Although the Jeans mass is well-resolved in this calculation, we did not observe the formation of any new stars. This is due to the fact that a Jeans mass of $\sim 40 M_{\odot}$ represents a significant fraction of the cluster's total residual gas content and it is very difficult to gather such a large quantity of material into one place.

The competition between the constructive and destructive impacts of feedback seen in these simulations is also apparent in the behaviour of systems such as M16 and NGC 3603 in which the effects of massive stars on molecular clouds can be observed directly. Based on their observations of NGC 3603, Tapia et al. (2001) conclude that, while the cluster HD 97950 is evidently destroying its natal molecular cloud, the existence of embedded infrared objects near the ionisation fronts also implies that triggered star formation is in progress in NGC 3603. Hester et al. (1996) observe

that the erosion of the famous gas pillars in the Eagle nebula is 'fixing' the masses of the stars already formed by preventing them from accreting additional material, just as occurred in our SL-1 calculation. However, they also suggest that radiatively-driven implosion may be responsible for stimulating the formation of the young stars in M16. However, McCaughrean & Andersen (2002) show that only $\sim 15\%$ of the gaseous clumps in M16 (dubbed Evaporating Gaseous Globules - EGGS - by Hester et al. (1996)) contain infrared point sources indicative of young stars or protostellar objects. It is evident that the problem of induced star formation is a difficult one requiring much further study.

5 IMPACT OF GRAVITY AND CLOUD STRUCTURE ON THE EFFECTIVENESS OF FEEDBACK

The initial conditions of the calculations presented above are clearly very complex. It is obviously of interest to attempt to determine what influence the structure present in our model protoclusters had on their evolution. It was already remarked that the radial density profiles of the models resemble power-laws. Smoothing out over 4π steradians the mass in spherical shells centred on $r = 0$ revealed that all the model clusters could be well represented by density profiles of the form

$$\rho = \begin{cases} \rho_{core} & \text{for } r \leq r_{core} \\ \rho_{core}(r_{core}/r)^{-2} & \text{for } r_{cluster} > r > r_{core} \end{cases} \quad (2)$$

where $r_{core} \simeq 0.01r_{cluster}$.

We used a simple one-dimensional Lagrangian code to investigate the effect of the clouds' structures on their evolution. The code's input physics consisted of fluid dynamics, gravity and photoionisation (note that the self-gravity of the gas was included in the calculation of gravitational forces to give better consistency with our SPH simulations). This code was used to model the evolution of initially-static density profiles with the form of Equation 2 corresponding to the high- and low-density SPH calculations.

There are four important lengthscales inherent in this problem. The initial efficacy of photoionisation is determined by the *initial* Strömgren radius, R_s corresponding to the gas number densities in the cores of the smoothed clouds. The *maximum* efficacy of photoionisation is determined by the equilibrium Strömgren radius, R_{eq} at which the HII region would come into pressure equilibrium with the ambient gas if the ambient gas were of density ρ_{core} everywhere. In the absence of gravity, the subsequent evolution of the HII region would be determined purely by the size of R_s or R_{eq} relative to the third lengthscales of interest, the cloud core radius, r_{core} . The propagation of an ionisation front resulting from the sudden ignition of an ionising source in an initially stationary uniform medium passes through two phases (see e.g. Spitzer 1978). In the very early stages of the development of the HII region, the recombination rate inside the HII region is small compared with the photon output of the source and most of the photons emitted ionise fresh material at the ionisation front. The propagation speed of the front is highly supersonic and the timescale on which the HII region grows is much shorter than any relevant dynam-

Run	R_s (cm)	R_{eq} (cm)	R_{esc} (cm)	r_{core} (cm)
UH-1	2.0×10^{15}	3.4×10^{17}	5×10^{16}	3.8×10^{16}
SL-1	3.0×10^{16}	5.1×10^{18}	4×10^{15}	8.2×10^{16}

Table 2. Comparison of the important lengthscales in the high- and low-density calculations

ical timescales. The gas remains everywhere approximately motionless in this evolutionary phase, during which the ionisation front is termed an ‘R-type’ front. As the HII region grows, the radiation reaching the ionisation front becomes geometrically diluted and the recombination rate inside the HII region increases, eventually becoming comparable to the photon luminosity of the source. The propagation speed of the ionisation front therefore decreases continually. When the speed of the ionisation front becomes comparable to the sound speed in the HII region, the timescale on which fresh gas is ionised becomes longer than the sound-crossing time of the system and the HII region expands dynamically, driving a strong shock before it. The ionisation front is subsequently known as a ‘D-type’ front and is confined behind the shock front because, in a uniform medium, the shock is always able to sweep up enough material to confine the ionisation front. If the medium in which the ionising source is born is not uniform, but instead possesses a power-law density profile $\rho \sim \rho_{core}^{-w}$, this is not necessarily true. It can be shown that, in cored density profiles in which the density of the envelope falls off more steeply than $w = \frac{3}{2}$, if the HII region is able to expand beyond the core during either the initial R-type phase or the D-type phase, it will expand to infinite radius (Franco et al. 1990).

Most of the theoretical work on HII regions completed to date assumes the gas involved to be initially at rest and neglects the effects of the gravitational field of the radiation source. The addition of gravitational forces introduces a fourth lengthscale to the problem, which we term the gravitational escape radius, R_{esc} . This is the radius within which the escape velocity due to the gravitational field of the ionising source and of the gas itself exceeds the thermal velocity of the ionised gas. One might expect that an HII region which achieves ionisation equilibrium within this radius will not be able to expand.

We list in Table 2 the four lengthscales described above corresponding to the smoothed versions of the high- and low-density SPH calculations. In both cases, the initial Strömgren radii of the clouds are inside their core radii, so the HII regions in both calculations are expected to come into ionisation equilibrium and enter their D-type expansion phase before encountering the power-law slope in the density profiles. Also in both cases, the equilibrium Strömgren radii lie outside the core radii. In the absence of gravity, one would therefore expect the HII regions in both calculations to expand beyond the cores and to ionise the whole clouds. However, the clouds differ in that, in the high-density case, the initial Strömgren radius lies *inside* the gravitational escape radius, whereas in the low-density cloud, the reverse is true. This suggests that the HII region in the high-density cloud may be prevented from expanding, but that in the low-density cloud, the HII region should be able to overflow the core and to then engulf the whole cloud. Both pre-

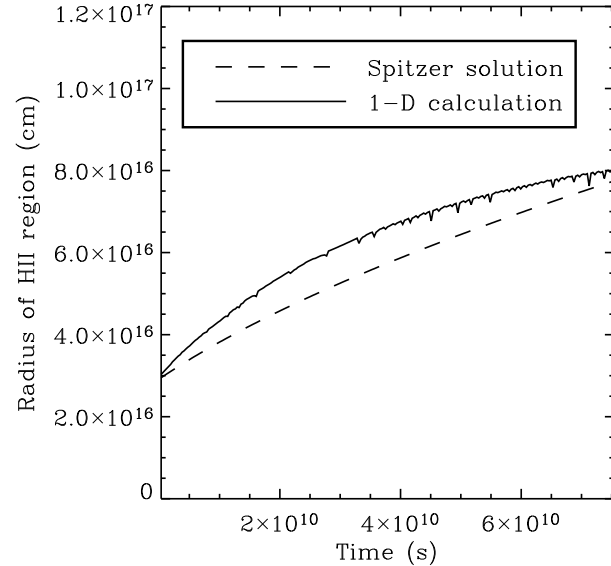


Figure 21. Comparison of the evolution of the HII region under the influence of gravity with the Spitzer solution.

dictions are borne out by the results from our one-dimension calculations. In the high-density case, the HII region had almost no effect on the dynamics of the gas, which rapidly settled into a steady freefall accretion flow. In the low density calculation, the expansion of the ionisation front is similar to the well-known Spitzer solution which would obtain in the absence of gravity in the uniform-density core of the cloud, given by

$$R(t) = R_s \left(1 + \frac{7}{4} \frac{c_s t}{R_s} \right)^{\frac{4}{7}}, \quad (3)$$

where c_s is the isothermal sound speed in the ionised gas.

The HII region in our calculation expands faster than the Spitzer solution as it accelerates down the density gradient generated by the accretion flow and rapidly reaches the core radius. Once it leaves the core, the HII region will expand rapidly to engulf the whole cloud.

We therefore find that gravity prevents the HII region expanding in the case where the Strömgren radius is well inside the escape radius, but indirectly accelerates the expansion for $R_s > R_{esc}$ by creating a density gradient.

The results of our one-dimensional calculations suggest that, if the UH-1 and SH-1 protoclusters investigated in Section 3 had not possessed a high degree of structure, the effect on them of the photoionising radiation from their central massive stars would have been negligible. However, it appears that the structure present in the SL-1 calculation lessened the effectiveness of feedback by preventing the source from ionising all the gas in the system, as the one-dimensional calculation suggests that it should. As one might expect, the ‘clumpiness’ of the gas makes the impact of photoionisation less dependent on the mean gas density.

These results have interesting implications for the problem of the energy source required to ionise the Diffuse Interstellar Gas (DIG) in spiral galaxies. The DIG exists as a layer of ionised hydrogen filling large volume fractions of spiral galaxies and accounting for up to 50% of their H α flux (Ferguson et al. (1996)). The Lyman continuum power

required to ionise the DIG is too large to be accounted for by winds or supernovae and the only remaining plausible source is the photoionising radiation from OB stars. In order to produce diffuse ionised gas, this radiation must be able to escape from HII regions. Our results show that this is indeed possible but that the quantity of radiation that can escape an HII region depends strongly on its internal structure. In our high-density simulations, the fractions of flux escaping the clouds towards the ends of the runs was $\sim 20\% (\sim 1.2 \times 10^{49} \text{ s}^{-1})$, whereas the HII region in the corresponding one-dimensional calculation was trapped within the cluster. It was therefore only due to the clumpiness of the gas that any radiation was able to escape the HII region. Conversely, in the low-density SPH simulations, $\sim 70\% (\sim 1.4 \times 10^{49} \text{ s}^{-1})$ of the flux was escaping by the end of the run. In the one-dimensional calculation, the cloud became fully ionised and the fraction of flux escaping would approach unity. The inhomogeneities in the gas therefore limited the escaping flux in the low-density calculations. Although the fluxes should be treated only as estimates, since the boundaries of our clouds were arbitrary, our results suggest that large fluxes of ionising photons can escape from HII regions and are thus a potential means of ionising the DIG. Reynolds in Lesch et al. (1997) calculates that $\sim 15-20\%$ of the total Lyman continuum from O-stars would be sufficient to ionise the DIG in the Galaxy, which our results demonstrate is feasible.

Our calculations also provide an interesting insight into the ultracompact HII region lifetime problem (Wood & Churchwell (1989)). Several authors (e.g. de Pree et al. (1995), Garcia-Segura & Franco (1996)) have suggested that the expansion of Ultra-Compact HII Regions (UCHIIRs) may be prevented by pressure confinement if the temperatures and number densities of the cores in which the HII regions form are somewhat higher than those typically assumed for molecular clouds or if additional magnetic or turbulent pressures are present. The expansion of the HII regions in our SPH calculations is indeed strongly affected by dynamical pressure, namely the ram-pressure of the accretion flows delivering gas into the vicinity of the radiation source. However, because these ram-pressures are highly anisotropic, they only hinder or prevent expansion of the HII region in some directions, leading to the complex geometry shown in Figure 7. Our one-dimensional calculations also suggest that the gravitational field of the source may be able to prevent HII region expansion.

Koo et al. (1996) and Kurtz et al. (1999) both conducted surveys of UCHIIRs in which they found evidence for extended emission around many sources which are regarded as compact. If it can be shown that such extended emission is directly related to the compact sources, this may alleviate the lifetime problem since it implies that the HII regions *have* expanded as expected. However, the source of the clumps of high-density ionised gas embedded within extended, lower-density HII remains a problem. This topic is discussed by Franco et al. (2000), who suggest that the clumps may be formed by instabilities during the formation or expansion phase of the HII region. We suggest another possibility. The densest ionised gas in our simulations is located at the tips of the filamentary accretion flows and is visible in Figure 7 as the small white region at the centre of the image. Although this very dense material is constantly

being accreted, it is also constantly being replenished by the accretion flows, so the small region of very dense ionised gas near the source will persist for as long as the accretion flows.

The interaction of HII regions with accretion flows in the presence of gravitational fields is evidently a problem which requires a great deal of further study.

6 CONCLUSIONS

We have undertaken the first ever hydrodynamic simulations of star cluster formation that incorporate feedback from ionising radiation from massive stars. These simulations differ from preceding feedback simulations (e.g. Tenorio-Tagle et al. 1986) in that the initial gas density distribution has the highly complex morphology that one would expect to develop in the gravitationally unstable regions of molecular clouds. In particular, the ionising source is located in the cluster core, close to the intersection of a number of dense, nearly radial filaments of inflowing gas. Our chief results are as follows:

(1) Radial filaments of gas in the cluster core provide a mechanism for collimating a number of outflows from the vicinity of the massive star. The opening angles, flow velocities and mass-loss rates compare very favourably with those of observed outflows in regions of massive star formation. A more detailed analysis is required in order to assess what fraction of outflows can be collimated by the gaseous environment in this way, compared with the number of sources that require an intrinsic collimation mechanism close to the star.

(2) The simulations demonstrate both positive and negative feedback effects. Ionisation reduces the rate of inflow of gas into the cluster core and thus reduces the growth rate of the most massive star compared with control simulations without feedback. On the other hand, feedback also enhances the production of *new* stars due to lateral compression of neutral gas in the walls separating adjacent ionised flows. The latter process is not fully resolved by our calculation, so we cannot at present quantify the relative importance of positive and negative feedback effects.

(3) We find that ionisation exacerbates small asymmetries in the initial gas distribution and rapidly generates grossly asymmetric gas structures (see Figures 4, 11 and 16). The impact of ionisation on the cloud (in terms of the volume-filling factor of ionised gas) can be greatly enhanced by the anisotropic gas distribution. The ‘damage’ inflicted by ionisation can readily be assessed from figure 11. By contrast, if the same ionising source is ignited in a cluster whose gas distribution was an azimuthally-averaged rendition of the gas distribution we employ here, we find that the ionising region would be completely trapped within the cluster core (i.e. within ~ 0.02 pc of the source). However, we also find that the impact of feedback can be decreased by such structure, as shown by comparing our SL-1 run with the corresponding azimuthally-averaged calculation, the latter suggesting that all the gas in the system should be ionised. Instead, the formation of high-density structures protects some of the gas in the system, at least temporarily, from the radiation field, allowing it to remain neutral.

(4) We find that although the gas in our simulations absorbs a quantity of thermal and kinetic energy from the ionising source that comfortably exceeds the gravitational binding energy of the cluster, this *is not* a good criterion for assessing whether the cluster will ultimately remain bound or not. The reason for this is simply that most of the energy is acquired by a relatively small fraction of the gas (i.e. that involved in the outflows) which is accelerated to a speed that significantly exceeds the cluster escape velocity and carries the energy out of the system.

(5) Because of the clumpy nature of the gas in our simulations, we found that significant fractions of our sources' ionising fluxes were able to escape our HII regions entirely, although whether the fraction escaping is enhanced or decreased by the structure of the gas depends on the mean gas density. Our results demonstrate that radiation leaking from HII regions is a plausible means of ionising the Diffuse Ionised Gas in spiral galaxies.

The above results suggest that the issue of unbinding clusters by photoionisation, and of the local Star Formation Efficiency in massive star-forming regions needs to be revisited. The fact that massive stars - in simulations and in reality - form in the cluster core where the gas is densest in general inhibits photoionisation feedback, although this effect may be mitigated by stellar wind clearing, which is not included in these simulations. As one would expect, density is the key parameter that controls the efficiency of feedback (contrast Figure 11 with Figure 16). This suggests that there are certain areas of mass-radius parameter space for protoclusters' progenitor clouds which allow the runaway growth of massive stars in the cluster core. Thus - quite apart from the issue of whether massive stars form by coalescence or accretion - the density dependence of feedback provides an additional reason why the most massive stars form in the densest cluster environments.

ACKNOWLEDGMENTS

We gratefully acknowledge the anonymous referee for very helpful comments. JED acknowledges support from a PPARC studentship. CJC gratefully acknowledges support from the Leverhulme Trust in the form of a Phillip Leverhulme prize. The computations reported in Section 3.1 were performed using the UK Astrophysical Fluids Facility (UKAFF).

REFERENCES

Adams, F. C. 2000, ApJ, 542, 964
 Arthur, S. J., Kurtz, S. E., Franco, J., & Albarrán, M. Y. 2004, ApJ, 608, 282
 Battinelli, P. & Capuzzo-Dolcetta, R. 1991, in ASP Conf. Ser. 13: The Formation and Evolution of Star Clusters, 139–141
 Beuther, H., Schilke, P., Gueth, F., et al. 2002, A&A, 387, 931
 Boily, C. M. & Kroupa, P. 2003, MNRAS, 338, 673
 Bonnell, I. A. & Bate, M. R. 2002, MNRAS, 336, 659
 Bonnell, I. A., Bate, M. R., & Zinnecker, H. 1998, MNRAS, 298, 93
 Churchwell, E. 1997, ApJL, 479, L59+
 Clarke, C. & Oey, M. S. 2002, MNRAS, 337, 1299
 Clarke, C. J., Bonnell, I. A., & Hillenbrand, L. A. 2000, Protostars and Planets IV, 151
 Davis, C. J., Varricatt, W. P., Todd, S. P., & Ramsay Howat, S. K. 2004, A&A, 425, 981
 de Pree, C. G., Rodriguez, L. F., & Goss, W. M. 1995, Revista Mexicana de Astronomia y Astrofisica, 31, 39
 Dekel, A. & Silk, J. 1986, ApJ, 303, 39
 Diaz-Miller, R. I., Franco, J., & Shore, S. N. 1998, ApJ, 501, 192
 Edgar, R. & Clarke, C. 2003, MNRAS, 338, 962
 Edgar, R. & Clarke, C. 2004, MNRAS
 Elmegreen, B. G. 1998, in ASP Conf. Ser. 148: Origins, 150–+
 Elmegreen, B. G. 2000, ApJ, 530, 277
 Elmegreen, B. G., Palouš, J., & Ehlerová, S. 2002, MNRAS, 334, 693
 Ferguson, A. M. N., Wyse, R. F. G., Gallagher, J. S., & Hunter, D. A. 1996, AJ, 111, 2265
 Franco, J. & Garcia-Segura, G. 1996, Bulletin of the American Astronomical Society, 28, 848
 Franco, J., Kurtz, S. E., Garcia-Segura, G., & Hofner, P. 2000, ApSS, 272, 169
 Franco, J., Tenorio-Tagle, G., & Bodenheimer, P. 1990, ApJ, 349, 126
 Garcia-Segura, G. & Franco, J. 1996, ApJ, 469, 171
 Geyer, M. P. & Burkert, A. 2001, MNRAS, 323, 988
 Goodwin, S. P. 1997, MNRAS, 284, 785
 Hartmann, L. 2003, ApJ, 585, 398
 Hegmann, M. & Kegel, W. H. 2003, MNRAS, 342, 453
 Hester, J. J., Scowen, P. A., Sankrit, R., et al. 1996, AJ, 111, 2349
 Hills, J. G. 1980, ApJ, 235, 986
 Hobson, M. P. & Padman, R. 1993, MNRAS, 264, 161
 Hobson, M. P. & Scheuer, P. A. G. 1993, MNRAS, 264, 145
 Kessel-Deynet, O. & Burkert, A. 2000, MNRAS, 315, 713
 Klein, R. I., Fisher, R. T., Krumholz, M. R., & McKee, C. F. 2003, in Revista Mexicana de Astronomia y Astrofisica Conference Series, 92–96
 Koo, B., Kim, K., Lee, H., Yun, M., & Ho, P. T. P. 1996, ApJ, 456, 662
 Kumar, M. S. N., Bachiller, R., & Davis, C. J. 2002, ApJ, 576, 313
 Kurtz, S. E., Watson, A. M., Hofner, P., & Otte, B. 1999, ApJ, 514, 232
 Lada, C. J., Margulis, M., & Dearborn, D. 1984, ApJ, 285, 141
 Lesch, H., Dettmar, R., Mebold, U., & Schlickeiser, R., eds. 1997, The Physics of Galactic Halos
 McCaughrean, M. J. & Andersen, M. 2002, A&A, 389, 513
 McKee, C. F. 1989, ApJ, 345, 782
 McKee, C. F. & Ostriker, J. P. 1977, ApJ, 218, 148
 Röllig, M., Hegmann, M., & Kegel, W. H. 2002, A&A, 392, 1081
 Shaviv, N. J. 2001, MNRAS, 326, 126
 Shepherd, D. S., Churchwell, E., & Wilner, D. J. 1997, ApJ, 482, 355
 Spitzer, L. 1978, Physical processes in the interstellar medium (New York Wiley-Interscience, 1978. 333 p.)

Tapia, M., Bohigas, J., Pérez, B., Roth, M., & Ruiz, M. T. 2001, Revista Mexicana de Astronomia y Astrofisica, 37, 39

Tassis, K., Abel, T., Bryan, G. L., & Norman, M. L. 2003, ApJ, 587, 13

Tenorio-Tagle, G., Bodenheimer, P., Lin, D. N. C., & Noriega-Crespo, A. 1986, MNRAS, 221, 635

Tenorio-Tagle, G., Palouš, J., Silich, S., Medina-Tanco, G. A., & Muñoz-Tuñón, C. 2003, A&A, 411, 397

Tenorio-Tagle, G., Silich, S. A., Kunth, D., Terlevich, E., & Terlevich, R. 1999, MNRAS, 309, 332

Whitworth, A. 1979, MNRAS, 186, 59

Whitworth, A. P. & Francis, N. 2002, MNRAS, 329, 641

Witt, A. N. & Gordon, K. D. 1996, ApJ, 463, 681

Wolfire, M. G. & Cassinelli, J. P. 1986, ApJ, 310, 207

Wolfire, M. G. & Cassinelli, J. P. 1987, ApJ, 319, 850

Wood, D. O. S. & Churchwell, E. 1989, ApJS, 69, 831

Yorke, H. W. & Sonnhalter, C. 2002, ApJ, 569, 846

Yorke, H. W., Tenorio-Tagle, G., Bodenheimer, P., & Rozycka, M. 1989, A&A, 216, 207

Zuckerman, B. & Evans, N. J. 1974, ApJL, 192, L149